# Transmission line based thermoacoustic imaging of small animals

Murad Omar<sup>1</sup>, Stephan Kellnberger<sup>1</sup>, George Sergiadis<sup>2</sup>, Daniel Razansky<sup>1</sup> and Vasilis Ntziachristos<sup>1</sup>

<sup>1</sup>Institute for Biological and Medical Imaging, Technische Universität München and HelmholtzZentrum München

<sup>2</sup>Department of Electrical and Computer Engineering, Aristotlte University of Thessaloniki

e-mail address:murad.omar@tum.de

**Abstract:** We have generated high resolution images of RF-Contrast in small animals using near-field thermoacoustic system. This enables us to see some anatomical features of a mouse such as the heart, the spine and the boundary.

OCIS codes: (000.0000) General; (000.0000) General [8-pt. type. For codes, see <a href="www.opticsinfobase.org/submit/ocis.">www.opticsinfobase.org/submit/ocis.</a>]

#### 1. Introduction

RF induced thermoacoustics is the generation of ultrasound waves using ultrashort pulses of radio waves or microwaves, because of the higher penetration depth of radio waves in comparison to the visible and infrared light, thermoacoustics is more suitable for clinical applications than optoacoustics is. The use of the thermoacoustic effect for biomedical imaging was first proposed by Theodor Bowen in 1981[1]. Although the methodology was proposed in the paper of Bowen in 1981, no imaging experiments were performed until 1999, because the necessary technology including ultrasonic transducers, efficient RF/microwave generators, and suitable acquisition systems were not widely available at that time. In 1999 Kruger et. al. designed a system for imaging breast cancer using this phenomenon at 434MHz[2, 3], then in the same year Lihong Wang managed to generate thermoacoustic images of biologically mimicking phantoms and biological samples at 3GHz using the same phenomenon[4-6]. Pulse modulated RF/microwave generators at 434MHz and 3GHz were used respectively at pulse widths as long as 0.5µs, this long pulse acted as a low pass filter on the generated ultrasound frequencies, thus limiting the resolution[7], in both cases a resolution of 1mm was achieved [2, 6].

To overcome this problem Razansky et. al. proposed in 2010 the use of broadband high energy RF-pulses[8], in his work Razansky used an impulse generator to generate short broadband RF pulses, later on Kellnberger et. al. used this method to image small animals *ex-vivo*[9]. In 2012 Omar et. al. developed the 2<sup>nd</sup> generationg of this system, the impulse generator was redesigned in such a way that the energy generated is decoupled from the length of the pulse by using transmission lines instead of normal capacitors [10, 11]. In this proceeding first the theory of thermoacoustic generation and the generation of RF-broadband pulses is explained, then the experimental setup is described, finally the results are shown and discussed at the end.

### 2. Theory

The generation of the thermoacoustic signals is based upon the thermoacoustic effect where an ultrasonic wave is generated inside a material due to the absorption of electromagnetic energy. The generated pressure is governed by the thermoacoustic wave equation[10]:

$$\nabla^{2} p(\vec{r}, t) - \frac{1}{v_{s}^{2}} \frac{\partial^{2} p(\vec{r}, t)}{\partial t^{2}} = -C \frac{\partial P_{loss, D}(\vec{r}, t)}{\partial t}$$
(1)

Where C is a constant, and  $P_{loss,D}$  is the amount of the electromagnetic energy absorbed inside the material, in the case of stress and thermal confinement and a homogeneous field distribution time and space variables in  $P_{loss,D}$  could be separated[12]. Moreover in the frequency range below 100MHz the energy absorbed is mostly dependent on the strength of the electric field and on the conductivity of the imaged material, such that the losses could be described as[10]:

$$P_{loss,D}(\vec{r},t) \approx \sigma(\vec{r}) |\vec{E}(t)|^2$$
 (2)

Opto-Acoustic Methods and Applications, edited by Vasilis Ntziachristos, Charles P. Lin, Proc. of OSA Biomedical Optics-SPIE Vol. 8800, 88000D · © 2013 OSA-SPIE CCC code: 1605-7422/13/\$18 · doi: 10.1117/12.2032561

Proc. of OSA-SPIE Vol. 8800 88000D-1

Different tissues has different conductivities[13], for example muscle has a much higher conductivity than fat does, tumor tissues also have a high conductivity in comparison to normal tissues, based on this different tissues dissipate RF energy in a different quantities, which generates the contrast in a thermoacoustic image.

The resolution of the generated image is dependent on the width of the excitation pulse[7], and the amplitude of the generated pressure signals is dependent on the amount of the energy coupled to the medium, when using an ordinary high voltage capacitor both of them are coupled together, thus to make the pulse shorter the amount of the energy coupled is less. On the other hand when using a transmission line as a medium for storing the energy the amount of the energy stored is decoupled from the width of the pulse. In this case the width of the pulse is given by:

$$\tau_{pulse} = 2 \frac{\ell_{line}}{c} \tag{3}$$

where  $\ell_{line}$  is the physical length of the transmission line, c is the propagation velocity of the electromagnetic wave inside the transmission line. In this case the amount of the energy is dependent on the capacitance of the transmission line:

$$E_0 = \frac{1}{2}CV^2 (4)$$

This energy could be increased either by increasing the charging voltage, or by increasing the number of transmission lines that are connected in parallel without compromising the width of the pulse!

Finally because the object is in the near field of the antenna, most of the energy is coupled to the object rather than radiated outside, hence the name near-field radio-frequency thermoacoustic tomography[8].

#### 3. Experimental Setup

The experimental setup that was employed in the studies was made of the impulse generator, a helix antenna for coupling the energy to the object, a rotation stage for acquiring measurements in a tomographic setup, a cylindrically focused ultrasound transducer for measuring the generated thermoacoustic signals and a data acquisition system.

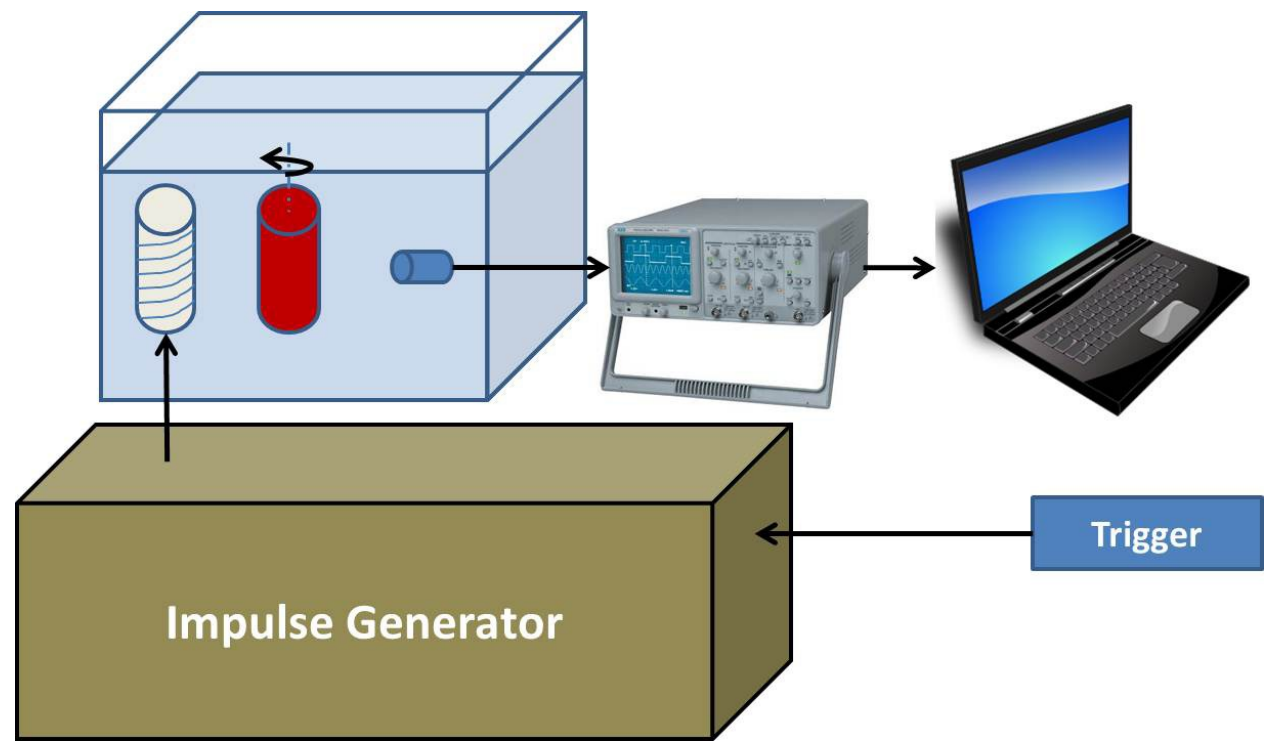


Fig. 1: Measurement setup, the basic parts such as the impulse generator, the antenna, the ultrasonic transducer and the data acquisition system appear here.

The impulse generator consists of high voltage coaxial cables (167-8556, Teledyne Reynolds), a high voltage source for charging the transmission lines (30C24-N124, HVProducts, USA), as well as a spark-gap capable of switching tens of kV's within nanoseconds. The helix antenna is a house made antenna and it is connected to the output of the pulser. The rotational stage is a commercially available rotation stage (PRM1Z8, Thorlabs Inc.), it rotates the imaged object 360° to generate tomographic images. The ultrasound transducer is also a commercially available cylindrically focused transducer (V382, Panametrics, Olympus NDT, USA) which has a center frequency of 3.5MHz and bandwidth of 70%, the signals are amplified using a low noise amplifier (63dB, Miteq Inc, USA), and finally digitized using an oscilloscope (TDS3054B, Tektronix Inc., USA), all of this was controlled from within MATLAB (Mathworks Inc., Natick, MA, USA). The system could be seen in Fig. 1.

The object was placed in the near vicinity of the helix antenna, this allowed for a maximum energy coupling between the antenna and the object. To minimize the jitter between the acquisition and the generation of the RF-pulses an electric field probe was used, then the oscilloscope was triggered on the rising edge of the electric field.

The core of the system is the transmission line based impulse generator, the trigger signal was amplified in the triggering circuitry, then the trigger was used to close the switch, the switch is a high voltage fast spark gap, and the impulse generator is sketched in Fig. 2.

The measured signals were reconstructed into images using the delay and sum algorithm[10], where at each reconstructed pixel the contributions from all the detectors was calculated by applying appropriate time delays to the signals, furthermore to decrease the effect of acoustic reflections the signals were weighted statistically[14], this was done by giving more weight to the signals that arrive earlier to the transducer, thus decreasing the probability of summing signals that were reflected or scattered.



Fig. 2: the transmission line based impulse generator.

## 4. Results and discussion

First the pulse width generated using the impulse response was measured, this was done at the output of the impulse generator, for this a high voltage probe was used (PHV 4002-3, PMK GmbH, Germany), the results are shown in *Fig. 3*. In the figure we could see that the pulse width could go as low as 10ns, also it could be observed that it is possible to excite frequencies as high as 40MHz by varying the length of the transmission lines used. The pulser was capable of generating high voltage pulses at a rate of 20Hz limited by the output power of the charging high voltage source.

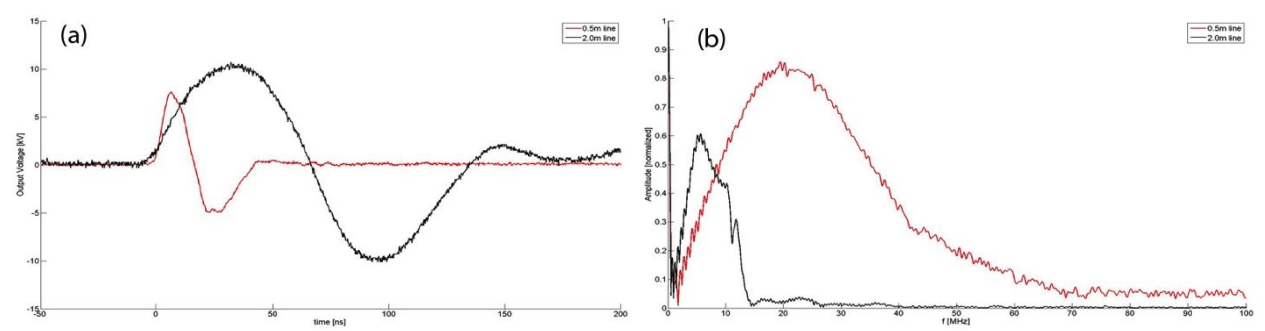


Fig. 3: Pulse generated with different lengths of transmission lines (a) Time-Domain Measurements, (b) Fourier transform of the measured impulses.

From Fig. 3 the variation of the pulse width with the length of the transmission line is seen, because of the use of transmission lines such short pulses as 10ns could be achieved.

This system was then used to image phantoms and mice *ex-vivo*, for the experiments 3 transmission lines each of length 2m were connected in parallel, the object was placed on a rotational stage, and 180 projections through 360° were made, at each position the signal was averaged 16 times to increase the SNR. As mentioned previously the delay and sum algorithm was used to reconstruct the images. Fig. 4 shows a phantom and two sections from a mouse, one from the abdomen region, and another one from the thorax region.

In Fig. 4(a) a tissue mimicking phantom is imaged, one tube was filled with deionized water and the other two tubes were filled with biological saline, a high difference in contrast between the different tubes could be seen in the figure, the ones filled with saline represent tissues with high electrical conductivity such as muscles, while the one filled with deionized water represents tissues with low conductivity such as fat.

Fig. 4(b,c) shows two tomographic sections from a mouse, one from the thorax region Fig. 4(b), and one from the abdomen region Fig. 4(c). In both the sections the boundary of the mouse could be seen, from the thorax region the heart, the spinal cord, the lungs, the muscles in the back of the mouse, and the ribs could be seen, while in the one from the abdomen, the boundary, an inner boundary, and the intestines could be seen.

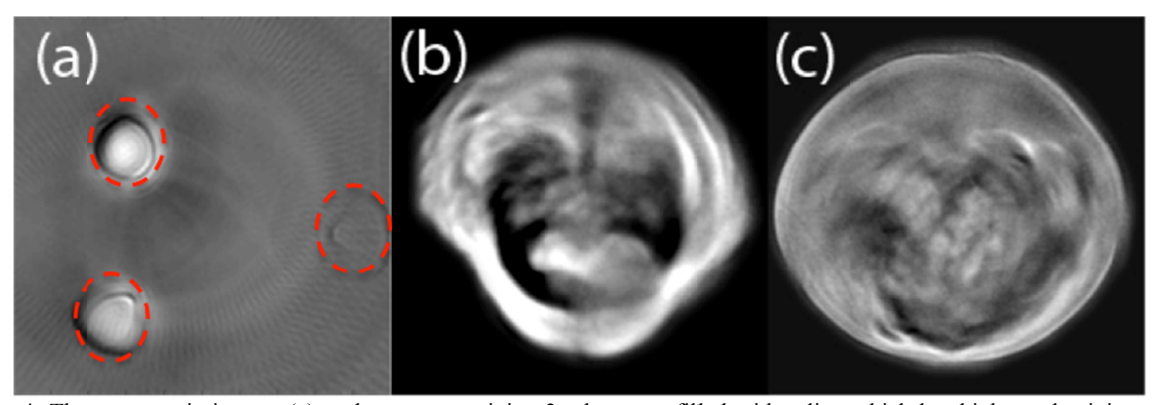


Fig. 4: Thermoacoustic images (a) a phantom containing 3 tubes, two filled with saline which has high conductivity, and one filled with deionized water. (b) thermoacoustic image from the thorax of a mouse, and (c) thermoacoustic image from the abdomen of the mouse.

In the future we are planning to increase the amount of the energy coupled to the sample for a higher SNR, we are planning also to increase the measurement time by switching the impulse generator at a higher pulse repetition rate, this is of interest for *in-vivo* studies of small animals.

#### 5. References

- 1. T. Bowen, "Radiation-Induced Thermoacoustic Soft Tissue Imaging," in IEEE Ultrasonic Symposium, (1981).
- R. A. Kruger, W.L. Kiser Jr, D. R. Reinecke, G. A. Kruger, R. L. Eisenhart, "Thermoacoustic Computed Tomography of the Breast at 434 MHz," IEEE MTT-S Digest (1999).

- 3. R. A. Kruger, K.D. Miller, Handel E. Reynolds, William L. Kiser, Daniel R. Reinecke, Gabe A. Kruger, "Breast Cancer in Vivo: Contrast Enhancement with Thermoacoustic CT at 434MHz-Feasibility Study," Radiology **216**, 279-283 (2000).
- Dazi Feng, Y. Xu, Geng Ku, Lihong V. Wang, "Microwave-induced thermoacoustic tomography: reconstruction by synthetic aperture," Medical Physics 28, 2427-2431 (2001).
- Geng Ku, L.V. Wang, "Scanning microwave-induced thermoacoustic tomography: Signal, resolution, and contrast," Medical Physics 28, 4-10 (2000).
- L. V. Wang, X. Zhao, Haitao Sun, and Geng Ku, "Microwave-induced acoustic imaging of biological tissues," Review of Scientific Instrumentation 70, 3744-3748 (1999).
- G. J. Diepold, T. Sun, M. I. Khan, "Photoacoustic Monopole Radiation in One, Two, and Three Dimensions," Physical Review Letters 67, 3384-3387 (1991).
- 8. Daniel Razansky, Stephan Kellnberger, and Vasilis Ntziachristos, "Near-field radiofrequency thermoacoustic tomography with impulse exciation," Medical Physics 37, 4602-4607 (2010).
- Stephan Kellnberger, Amir Hajiaboli, Daniel Razansky and Vasilis Ntziachristos, "Near-field thermoacoustic tomography of small animals," Physics in Medicine and Biology 56, 3433-3444 (2011).
- 10. Murad Omar, Stephan Kellnberger, George Sergiadis, Daniel Razansky, Vasilis Ntziachristos, "Near-field thermoacoustic imaging with transmission line pulsers," Medical Physics **39**, 4460-4466 (2012).
- Murad Omar, Stephan Kellnberger, George Sergiadis, Daniel Razansky, Vasilis Ntziachristos, "Near-field radio-frequency thermo-acoustic imaging based on transmission lines for optimized performance.," in (Proc. of SPIE, 2012), 822310-82231.
- 12. L. V. Wang, H.I. Wu, Biomedical Optics: Principles and Imaging (Wiley Interscience, 2007).
- 13. S Gabriel, R.W. Lau, C Gabriel, "The dielectric properties of biological tissues: III. Parametric models for the dielectric spectrum of tissues," Physics in Medicine and Biology 41, 2271-2293 (1996).
- XL Dean-Ben, R. Ma, D. Razansky, Vasilis Ntziachristos, "Statistical approach for optoacoustic image reconstruction in the presence of strong acoustic heterogeneities," IEEE transactions on medical imaging 30, 401-408 (2011).